Kütahya Dumlupınar University
Institute of Graduate Studies

Journal of Scientific
Reports-A
E-ISSN: 2687-6167
Number 52, March 2023

RESEARCH ARTICLE

FACILE AND CONTROLLED SYNTHESIS OF 2D ORGANOMETAL HALIDE PEROVSKITE PURE $BA_2MAPb_2I_7$ AND HETEROSTRUCTURED $BA_2PbI_4/BA_2MAPb_2I_7$ SINGLE CRYSTALS

Alp YILMAZ[1,*], Aydan YELTİK[2]

[1*]TOBB University of Economics and Technology, Department of Material Science and Nanotechnology Engineering, Ankara, alpyilmaz9898@gmail.com, ORCID: 0000-0002-5224-423X
[2]TOBB University of Economics and Technology, Department of Material Science and Nanotechnology Engineering, Ankara, ayeltik@etu.edu.tr, ORCID: 0000-0001-6976-4680

Receive Date:17.02.2023 *Accepted Date: 15.03.2023*

ABSTRACT

Two dimensional (2D) organometal halide perovskites (OHPs) have attracted intensive interest for their diverse optoelectronic applications. However, a practical and controllable solution-based way particularly for the synthesis of pure $BA_2MAPb_2I_7$ and heterostructured $BA_2PbI_4/BA_2MAPb_2I_7$ single crystals, which are of great importance for high performance photodetectors, is still lacking. In this study, we report the efficient synthesis route of large-area high-quality $BA_2MAPb_2I_7$ and $BA_2PbI_4/BA_2MAPb_2I_7$ single crystals. We show that the combined method of solution temperature lowering and limiting reagent approaches yields rapid and controllable synthesis. In addition, the correct determination of the BAI:MAI:PbI_2 molarity ratios in the synthesis process was revealed to be highly significant. These results provide fundamental insight and useful guideline for obtaining the presented 2D OHPs with regard to high practicality and controllability.

Keywords: *2D Perovskite, Single crystal synthesis, Solution temperature lowering, Limiting reagent approach, Heterostructure.*

1. INTRODUCTION

Among many prominent two dimensional (2D) materials such as graphene[1] and transition metal dichalcogenides (TMD)[2–4], 2D organometal halide perovskites (OHPs) are promising layered materials for optoelectronic applications owing to their favorable properties such as high carrier mobility, long diffusion length, high absorption coefficient, tunable optical bandgap, and ease of forming heterostructures with other materials[5,6]. 2D OHPs structures are generally defined by the chemical formula $(RNH_3)_2(A)_{n-1}MX_{3n+1}$, where RNH_3 is a long-chain organic group ($CH_3(CH_2)_3NH_3$, $C_6H_5C_2H_4NH_3$, etc.), A is an organic or inorganic cation ($CH_3NH_3^{+1}$, Cs, etc.), M is a bivalent metal cation (mainly Pb^{+2}, Sn^{+2}, Ge^{+2}, etc.), X is a halogen anion (Cl^-, Br^-, I^-). Here the n value represents the number of the inorganic octahedron layers, giving the inorganic layer thickness. In recent years, 2D

JSR A
Journal of Scientific Reports

OHPs have been studied as solution-processable active and supporting components in photovoltaics, LEDs, and photodetectors due to the higher stability feature compared to 3D OHPs and other superior characteristics[7].Particularly, long-chain hydrophobic organic groups increase the durability of 2D OHPs by protecting the inorganic octahedra layers[8,9]. Also, the optoelectronic properties of 2D OHPs are able to be adjusted by just varying the number of inorganic layers (n)[10,11]. Among the various applications of 2D OHP single crystals which yield high crystallinity and less number of grain boundaries, photodetectors stand out, providing superior responsivity and short response rate[12,13].

Heterostructures emerge as structures formed by the combination of two different semiconductor materials with different unique optoelectronic properties such as graphene, TMD, black phosphorus, and perovskite. Thus, heterostructures significantly increase the functionality of optoelectronic applications such as photodetectors, photovoltaics, and transistors[14]. In particular, the synthesis of two different perovskite structures with different compositions as a single crystal is very important in order to overcome the problems such as the requirement of matching the lattice constant, and the formation of interface defects at the boundaries of materials[15]. Nowadays, researchers have succeeded in synthesizing various 2D perovskite heterostructures such as $(BA)_2PbI_4/(BA)_2PbBr_4$, $(PEA)_2PbI_4/(PEA)_2MAPb_2I_7$, $(2T)_2PbI_4/(2T)_2PbBr_4$, $(2T)_2SnI_4/(2T)_2PbI_4$[16]. Moreover, 2D OHP single-crystal heterostructures are of great importance for dual-band high-performance photodetectors due to the tunable optical bandgap allowing high absorption coefficients over multiple spectral regions[15,17]. It is of great importance to synthesize high-quality 2D OHP pure single crystals and their heterostructures instead of widely used polycrystalline films for higher detector performances[15]. However, there are still important issues that need to be addressed and researched in detail regarding the synthesis process in terms of practicality and controllability. In particular, the use of slow and complex vapor deposition processes in the synthesis of $BA_2PbI_4/BA_2MAPb_2I_7$ single crystal heterostructures is a major concern.[18,19].

Single crystals of 2D OHPs with diverse optoelectronic properties have been obtained using compositional engineering through various synthesis methods such as solution-based crystal growth, vapor-phase epitaxial growth, and top-down (slicing, mechanical peeling) methods[20–22]. Among them, the solution-based crystal growth method is ideal for synthesizing 2D OHP single crystals with ease, high-quality and controllability[23]. Solution-based crystal growth methods are also listed as inverse temperature crystallization, anti-solvent vapor assisted crystallization, slow evaporation crystallization and solution temperature lowering (STL). The STL method is an important route for the synthesis of high-quality 2D OHP single crystals with large grain sizes[24]. On the other hand, during STL synthesis of 2D OHP $BA_2MAPb_2I_7$ (n=2) single crystal materials, which are of great importance for photodetector applications, BA_2PbI_4 (n=1) crystals are inevitably synthesized as side product and cause contamination; therefore, the inability to obtain homogeneous $BA_2MAPb_2I_7$ structures emerges as a major challenge[15]. Furthermore, this hinders the controlled synthesis of 2D OHP $BA_2PbI_4/BA_2MAPb_2I_7$ single crystal heterostructures for use in dual-band photodetectors. Considering the slow and complex vapor deposition processes used in the synthesis of $BA_2PbI_4/BA_2MAPb_2I_7$ single crystal heterostructures, a rapid and simple STL method provides highly important advantages for the controlled synthesis of heterostructures.

JSR A
Journal of Scientific Reports

In this study, high-quality, large-area, pure 2D OHP $BA_2MAPb_2I_7$ single crystals were synthesized within a few hours using a facile solution-based synthesis route. The high controllability of the used approach, which included STL and limiting reagent methods, was achieved by carefully varying the concentration ratios of n-butylamine (BA) and methylamine (MA) cations. 2D OHP $BA_2PbI_4/BA_2MAPb_2I_7$ single crystal heterostructures were also synthesized and investigated in detail. Structural and optical properties of the synthesized perovskites were examined using various characterization techniques including scanning electron microscopy/energy dispersive X-ray spectroscopy (SEM/EDX), X-ray diffractometry (XRD), UV-Vis absorption spectroscopy, and steady-state photoluminescence (PL) spectroscopy. Accordingly, the characteristic spectra of the $BA_2MAPb_2I_7$ and $BA_2PbI_4/BA_2MAPb_2I_7$ single crystals were obtained. The SEM images illustrated the synthesized single crystals having large-area and layered structures. The XRD pattern of $BA_2PbI_4/BA_2MAPb_2I_7$ single crystal heterostructures was obtained as a mixture of the patterns of $BA_2MAPb_2I_7$ and BA_2PbI_4 single crystals as targeted. This result was also obtained in the PL and UV-Vis absorption spectra.

2. EXPERIMENTAL SECTION

2.1. Chemicals

The chemicals used here in the synthesis of perovskites are lead(II) iodide (PbI_2), methylammonium iodide (MAI), n-butylamine (BA), 57% aqueous hydriodic acid (HI), 50% aqueous hypophosphorous acid (H_3PO_2). They were purchased from Sigma-Aldrich and used as received in high purity.

2.2. Growth of 2D OHP single crystals

STL and limiting reagent methods were utilized to synthesize 2D OHP $BA_2MAPb_2I_7$ single crystals. Schematics of the synthesis steps, including the parameters, are shown in Figure 1. Herein, the concentration ratio of BA cations has been limited in the synthesis process of pure $BA_2MAPb_2I_7$ 2D OHP single crystals. Accordingly, 1.32 M PbI_2 powder chemical was dissolved in 0.250 mL HI solvent (A solution). After stirring at 200 rpm for 10 minutes at the temperature of 90°C, a transparent yellow solution was obtained. After that, 0.66 M of MAI powder chemical was added to the solution and $MAPbI_3$ was formed, and the color of the solution turned dark black. After 10 minutes, 28 µL of H_3PO_2 was added to the solution, dissolved at 90°C under 150 rpm stirring for 2 hours and the color of the solution turned transparent yellow again.

In a separate flask placed in an ice bath, 0.86 M of n-BA was dissolved in 0.250 mL HI solvent to obtain BAI precursor solution (solution B). The n-BA was dropwise added and dissolved under stirring (200 rpm) at 0°C for 2 hours. An amount of solution B at 0°C was rapidly added to solution A at 90°C until observing red nuclei with hundreds of micron lateral areas. The temperature of the solution was increased to 100°C and stirred at 200 rpm for 15 minutes. The solution was cooled to 25°C at a cooling rate of 30°C/h and $BA_2MAPb_2I_7$ 2D OHP single crystals were grown. After that, the single crystals were collected by vacuum filtration and taken into vacuum for drying at 25°C overnight.

Further, BA_2PbI_4 2D OHP single crystals were synthesized using the STL method aforementioned, except that the molar concentrations of solution A and B were adjusted to the BAI:MAI:PbI_2 ratio of

JSR A
Journal of Scientific Reports

2:0:1. The synthesis of $BA_2PbI_4/BA_2MAPb_2I_7$ 2D OHP single crystal heterostructures was also carried out following the steps outlined above, but the concentrations of solution A and B were adjusted to the BAI:MAI:PbI_2 molarity ratios of 2:1:2, 2:2:2, 2:3:2 and 2:4:2.

2.3. Structural characterization

The basic properties of the materials such as crystal quality, surface morphology, lateral thickness and grain boundary identification of the materials were examined as preliminary characterization using an optical microscope (Nikon series Eclipse H600L). The XRD system (Bruker D8 Advance) operating at 40 kV and using Cu Kα (λ=1.5418Å) as X-ray source was employed to characterize the crystal structure of the materials and to determine the distance between the inorganic layers. The analysis was performed at room temperature and within the diffraction angle range of θ=4-60°, choosing 0.5 second/step and 0.01° step size. The SEM/EDX system (Phenom XL) was used to examine the material's morphology, grain orientation, grain size, layer thickness, chemical structure, different element maps on the surface, and element ratios in the materials. The SEM/EDX device was operated in point mode with 10 kV.

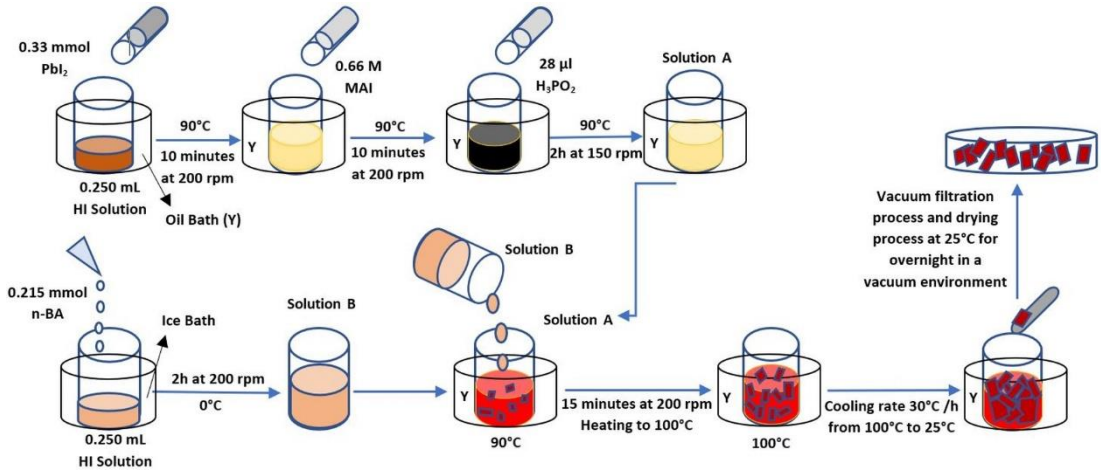

Figure 1. Schematic representation for the synthesis of 2D OHPs using STL method and limiting reagent approach.

2.4. Optical characterization

UV-Vis absorption spectroscopy was used to obtain the optical bandgap and absorption peak position of the synthesized materials. Hitachi U-5100 Spectrophotometer was operated in the wavelength range of 380-800 nm with a scanning speed of 100 nm/min. Cary Eclipse fluorescence spectrophotometer was used for the PL analyses to characterize the materials and reveal optical properties.

All the samples synthesized and investigated in this study were stored in Ar inert gas environment and all the characterization measurements were carried out at room temperature (25 °C).

JSR A
Journal of Scientific Reports

3. RESULTS AND DISCUSSIONS

High-quality $BA_2MAPb_2I_7$ 2D OHP single crystals with large surface area as shown in Figure 2(a-d) involving the SEM images with the corresponding EDX analyses were synthesized. The main principle of the utilized STL method is to obtain single crystals by gradually lowering the temperature. By this way, the solubility of perovskite decreases and a single crystal precipitate may form in saturated solution. The crystallization process takes place in two stages, nucleation, and crystal growth. The crystallization process begins with the formation of nucleation sites, which always occur in a supersaturated solution. The process can be controlled by adjusting the crystallization temperature and degree of saturation to maximize crystal growth and minimize co-nucleation to achieve the best single crystal quality. During the synthesis of $BA_2MAPb_2I_7$ 2D OHP single crystals, n=1 perovskites are synthesized as contamination[15]. This is because the solubility of perovskite single crystals in aqueous solution increases as the n value increases towards n=∞ while transforming from 2D to 3D[15,25,26]. Hence, BA_2PbI_4 2D OHPs were synthesized as the growth rate of BA_2PbI_4 (n=1) single crystals was higher than that of $BA_2MAPb_2I_7$ (n=2) single crystals. In addition, due to the higher solubility of MA cations in aqueous solution than BA cations, the inability of MA cations to reach supersaturation in the prepared solution led to a further decrease in the growth rate of $BA_2MAPb_2I_7$ 2D OHP single crystals[27]. Therefore, solutions A and B were prepared with the molarity ratio of BAI:MAI:PbI_2 adjusted to be 0.86:0.33:0.66. Limited amounts of BA cations in solution B are added to solution A until the color turning point is reached where red nuclei are observed, which is called the limiting reagent approach.

Furthermore, BA_2PbI_4 2D OHP single crystals were synthesized by adjusting the BAI:MAI:PbI_2 molarity ratios to be 2:0:1 considering the stoichiometric ratio, as seen from Figure 2(e-h). When the BAI:MAI:PbI_2 molarity ratio was adjusted to 2:1:2 by increasing the MAI concentration, BA_2PbI_4/$BA_2MAPb_2I_7$ 2D OHP single crystal heterostructures were synthesized, as shown in Figure 2(i-k). In addition, BA_2PbI_4/$BA_2MAPb_2I_7$ heterostructures were synthesized also by adjusting the BAI:MAI:PbI_2 molar ratios to 2:2:2, 2:3:2 or 2:4:2 by increasing the concentration of MA cations. Due to the excess amount of MA concentration, n=1 perovskite structure was synthesized as contamination and prevented the synthesis of n=2 perovskite structure by acting as a kinetic barrier[26]. The lateral dimensions of the successfully synthesized 2D OHP single crystals ranged from tens of micrometers to a few millimeters. SEM images in Figure 2 show that perovskite single crystals have a layered structure stacked on top of each other with a smooth and homogeneous surface morphology free from grain boundaries or voids. In addition, it was observed that a small part of the red nuclei with a lateral area of hundreds of microns at the beginning of the cooling process was on the interface of the solution, and a large part was at the bottom of the solution. The reason for this is that the nucleation energy barrier, defined as the threshold energy value that must be exceeded for nucleation to occur, is significantly lower at the liquid-air interface than inside the solution. Therefore, the nucleation occurs much more easily at the interphase boundary[27]. Accordingly, it was stated that hydrophilic BA ($C_4H_9NH_3^+$) precursor cations align at the liquid-air interphase boundary, acting as a template for nucleation, rather than binding to water molecules in solution via static Coulomb interaction.

JSR A
Journal of Scientific Reports

When the chemical analysis was made with the EDX method, the atomic concentration ratio of Pb:I in the structure of $BA_2MAPb_2I_7$ 2D OHP single crystals was found to be approximately 1:2, which is characteristic for the PbI_2 inorganic part of the perovskite structure. Moreover, while the weight concentrations of C and N atoms were found to be low, the weight concentrations of I and Pb atoms in the structure were found to be relatively high as shown in Figure 2(d). Previous studies have reported that perovskite structures are very sensitive to high-energy electron beams[28–32]. Therefore, these results are attributed to the increased temperature on the surface region in which high-energy electron beams are focused, causing the degradation of OHP single crystals. Accordingly, the organic part with higher volatility in the crystal structure is connected to the inorganic layers with weak van der Waals bonds. High thermal energy breaks the weak bonds and the organic volatile part splits from the structure. Owing to the same situation, similar results were observed for the BA_2PbI_4 and $BA_2PbI_4/BA_2MAPb_2I_7$ perovskites, as shown in Figure 2(h) and Figure 2(k), respectively.

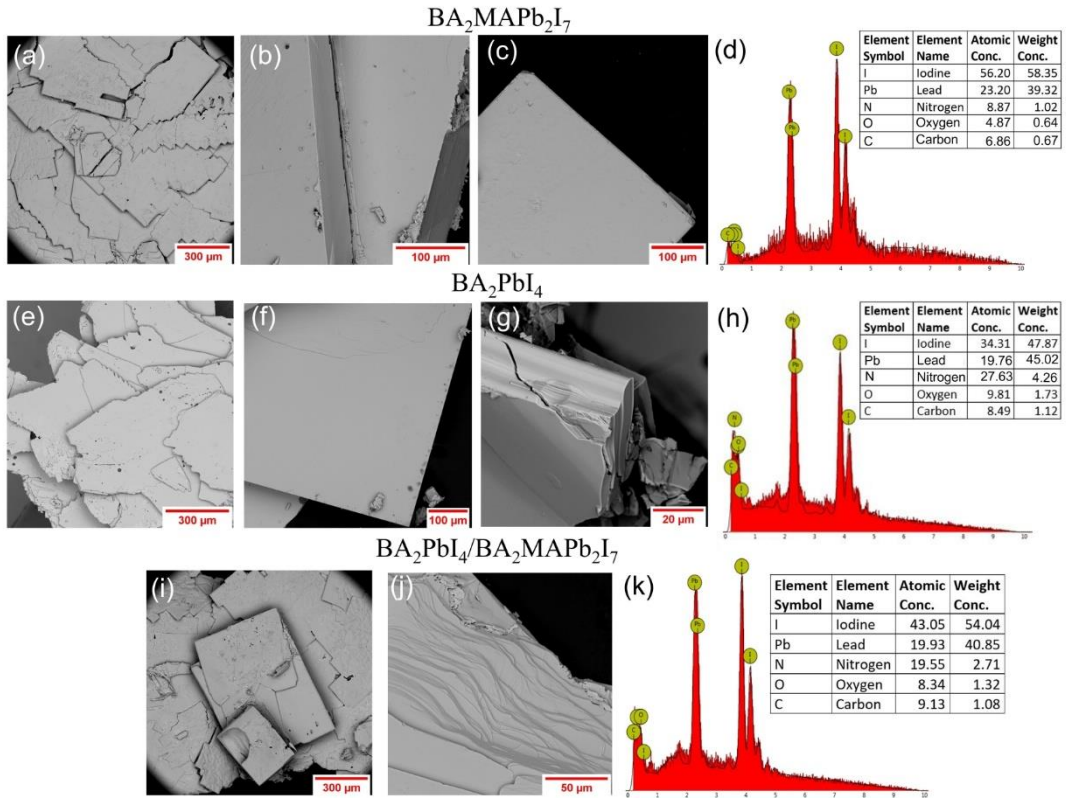

Figure 2. SEM images with the corresponding EDX spectra of the synthesized 2D OHP single crystals; **(a-d)** $BA_2MAPb_2I_7$, **(e-h)** BA_2PbI_4, and **(i-k)** $BA_2PbI_4/BA_2MAPb_2I_7$ heterostructure.

JSR A
Journal of Scientific Reports

Figure 3 shows comparative XRD patterns of BA_2PbI_4, $BA_2MAPb_2I_7$ 2D OHP single crystals and BA_2PbI_4/$BA_2MAPb_2I_7$ 2D OHP single crystal heterostructures. The characteristic crystal planes for the crystal structure of $BA_2MAPb_2I_7$ 2D OHP single crystals was determined at diffraction peaks of 4.6°, 9.14°, 13.67°, 18.23°, 22.83°, 27.43°, 32.1°, 36.86°, respectively. In the literature, Zhou et al. reported that high intensity XRD peaks of BA2MAPb2I7 crystals were obtained at the angles of 5.09°, 9.62°, 14.12°, 18.65°, 23.23°, 27.80° and 32.44°[33]. In addition, due to the continuity of the inorganic-organic-inorganic layer in the crystal structure of 2D OHP single crystals, the angle values at which XRD peaks increase regularly according to the d gap distance between the crystal planes[34–36]. Accordingly, the distance between the crystal planes of the synthesized 2D OHP single crystals was measured to be d=1.964nm and, using the Bragg equation ($n\lambda = 2dsin\theta$), it was calculated that the difference between the angle values between each peak should be approximately 2θ=4.5°, which is consistent with the obtained results. XRD analysis demonstrates a single crystallinity of perovskite structures and confirms that the 2D OHPs were successfully synthesized according to the XRD results in previous studies[26,37]. Furthermore, XRD analysis identified the diffraction peaks corresponding to the characteristic crystal planes of the BA_2PbI_4 2D OHP single crystals as 6.48°, 12.94°, 19.35°, 25.89°, 32.5°, 39.22°, respectively. In the literature, Zhou et al. reported that high intensity diffraction peaks at the XRD analysis of BA_2PbI_4 crystals were obtained at the angles of 7.01°, 13.45°, 19.91°, 26.44°, 33.06° and 39.79°[25]. These results are in agreement with the results of XRD analysis in previous studies confirming the synthesis of BA_2PbI_4 2D OHP single crystals[33,37]. In addition, XRD analysis of BA_2PbI_4/$BA_2MAPb_2I_7$ 2D OHP single crystal heterostructures includes each of the diffraction peaks for characteristic planes of the crystal structures of BA_2PbI_4 and $BA_2MAPb_2I_7$ 2D OHP single crystals. These results are also consistent with the XRD results of BA_2PbI_4 and $BA_2MAPb_2I_7$ 2D OHP single crystals in the literature[15,33].

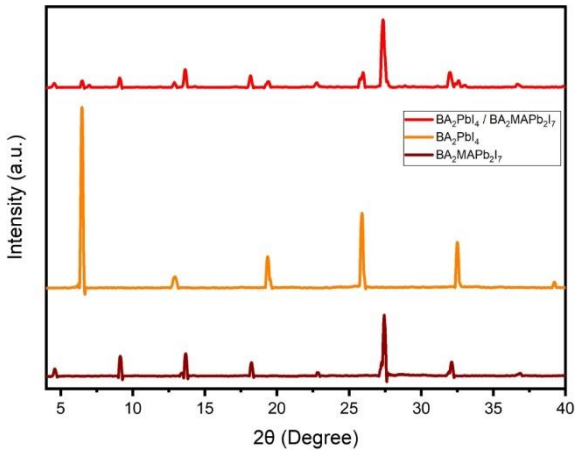

Figure 3. XRD patterns of the synthesized $BA_2MAPb_2I_7$, BA_2PbI_4, and BA_2PbI_4/$BA_2MAPb_2I_7$ single crystals.

Absorption spectroscopy (UV-Vis) analysis was also performed to examine the optical properties of $BA_2MAPb_2I_7$ 2D OHP single crystals and showed the absorption peak at about 576 nm as shown in

JSR A
Journal of Scientific Reports

Figure 4(a). Accordingly, there is a relationship between the photon energy ($(\alpha h\upsilon)^{1/n} = \beta(h\upsilon - E_g)$) and the absorption coefficient ($\alpha = \beta/(h\upsilon)\ (h\upsilon - E_g)^n$), and the band gap is determined by the straight line, which is drawn to the slope of the graph of $(\alpha h\upsilon)^{(1/2)}$ versus photon energy ($h\upsilon$). The optical bandgap value was calculated as 2.04 eV by using the Tauc plot drawn in the inset figure.

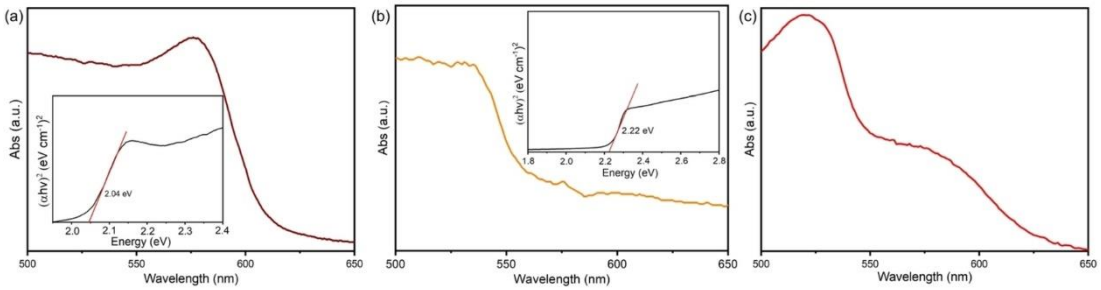

Figure 4. Absorption spectra of the synthesized single crystals; **(a)** $BA_2MAPb_2I_7$, **(b)** BA_2PbI_4, and **(c)** $BA_2PbI_4/BA_2MAPb_2I_7$ heterostructure. Insets show the corresponding Tauc plots.

In addition, it was analyzed that the absorption onset value extends towards longer wavelengths due to the trap states of the 2D OHP single crystals[38]. BA_2PbI_4 2D OHP single crystals have an absorption peak at about 535 nm, an absorption onset value extending up to 700 nm due to the quantum confinement effect, and an optical bandgap value of 2.22 eV, as shown in Figure 4(b). When the optical properties of the heterostructure were examined by UV-Vis characterization method, it was observed that it had two absorption peaks at about 535 nm for the BA_2PbI_4 perovskite structure and at about 576 nm for the $BA_2MAPb_2I_7$ perovskite structure, as shown in Figure 4(c).

The optical properties of perovskite single crystals were investigated using the PL characterization method. In Figure 5(a), it is observed that the center of the emission peak for $BA_2MAPb_2I_7$ 2D OHP single crystal is at a wavelength of 584 nm. In addition, in the PL spectrum plot of Figure 5(b), it is observed that single crystals have a single luminescence peak at 520 nm wavelength for BA_2PbI_4 2D OHP single crystals. In Figure 5(c), $BA_2PbI_4/BA_2MAPb_2I_7$ 2D OHP single crystal heterostructure PL spectrum shows that one of the PL peaks is centered at about 588 nm for $BA_2MAPb_2I_7$ and the other PL peak is for BA_2PbI_4 2D OHP single crystals. The gray dashed line in this figure represents the data that could not be obtained experimentally due to the filtering constraint of the instrument and was plotted considering the PL spectrum of BA_2PbI_4 OHP in Figure 5 (b).

JSR A
Journal of Scientific Reports

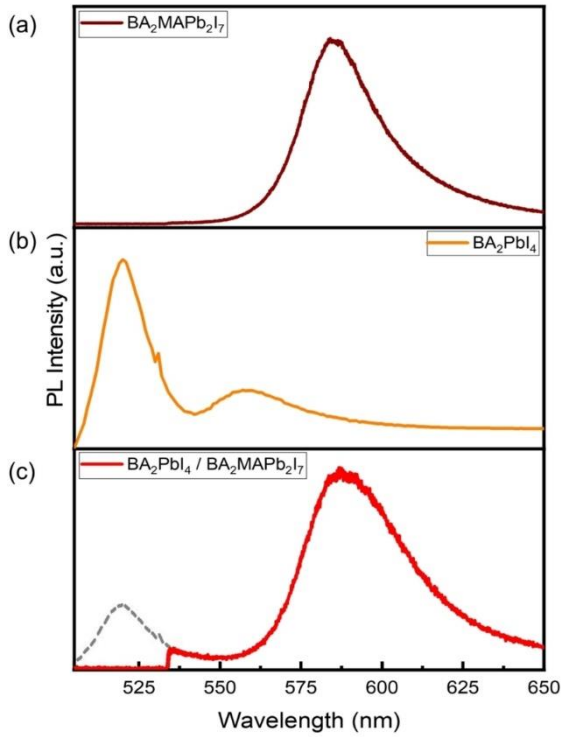

Figure 5. PL spectra of the synthesized single crystals; **(a)** $BA_2MAPb_2I_7$, **(b)** BA_2PbI_4, and **(c)** $BA_2PbI_4/BA_2MAPb_2I_7$ heterostructure.

4. CONCLUSION

In summary, large-area high-quality $BA_2MAPb_2I_7$ 2D OHP single crystals were able to be synthesized within a few hours using solution-based STL method and limiting reagent approach. The concentration ratio of BA and MA cations was revealed to be significant for the synthesis of these crystals. Accordingly, the synthesis of $BA_2PbI_4/BA_2MAPb_2I_7$ 2D OHP single crystal heterostructures was carried out successfully. Herein, various characterization methods were utilized to investigate structural and optical properties of the synthesized 2D OHP single crystals. A novel pathway was introduced on rapid and controllable synthesis of large-area high-quality $BA_2MAPb_2I_7$ and $BA_2PbI_4/BA_2MAPb_2I_7$ 2D OHP single crystals. It is of great importance to carry out such studies in order to develop new synthesis approaches of 2D OHP materials with superior properties for use in optoelectronic applications.

ACKNOWLEDGEMENT

This work was supported by Scientific and Technological Research Council of Turkey. Project Number: TÜBİTAK 121M601.

REFERENCES

[1] Tiwari, S.K., Sahoo, S., Wang, N. and Huczko, A., (2020), Graphene research and their outputs: status and prospect, Journal of Science: Advanced Materials and Devices, 5, 10–29.

[2] Aras, F.G., Yilmaz, A., Tasdelen, H.G., Ozden, A., Ay, F., Perkgoz, N.K. and Yeltik, A., (2022), A review on recent advances of chemical vapor deposition technique for monolayer transition metal dichalcogenides (MX2: Mo, W; S, Se, Te), Materials Science in Semiconductor Processing, 148, 106829.

[3] Aras, F.G., Avad, J. and Yeltik, A., (2022), Glass- Assisted Chemical Vapor Deposition- Grown Monolayer MoS2 : Effective Control of Size Distribution via Surface Patterning, Physica Status Solidi (A), 219, 2200503.

[4] Aras, F.G. and Yeltik, A., (2022), Role of gas flow direction on monolayer MoS2 growth on patterned surfaces via CVD, Semiconductor Science and Technology, 38, 015013.

[5] Hong, K., Le, Q. Van, Kim, S.Y. and Jang, H.W., (2018), Low-dimensional halide perovskites: review and issues, Journal of Materials Chemistry C, 6, 2189–2209.

[6] Quan, L.N., Rand, B.P., Friend, R.H., Mhaisalkar, S.G., Lee, T.-W. and Sargent, E.H., (2019), Perovskites for next-generation optical sources, Chemical Reviews, 119, 7444–7477.

[7] Chen, Y., Sun, Y., Peng, J., Tang, J., Zheng, K. and Liang, Z., (2018), 2D ruddlesden-popper perovskites for optoelectronics, Advanced Materials, 30, 1703487.

[8] Smith, I.C., Hoke, E.T., Solis-Ibarra, D., McGehee, M.D. and Karunadasa, H.I., (2014), A layered hybrid perovskite solar-cell absorber with enhanced moisture stability, Angewandte Chemie International Edition, 53, 11232–11235.

[9] Cao, D.H., Stoumpos, C.C., Farha, O.K., Hupp, J.T. and Kanatzidis, M.G., (2015), 2D homologous perovskites as light absorbing materials for solar cell applications, Journal of the American Chemical Society, 137, 7843–7850.

[10] He, J., Fang, W.-H. and Long, R., (2020), Two-dimensional perovskite capping layer simultaneously improves the charge carriers lifetime and stability of MAPbI3 perovskite: a time domain ab initio study, The Journal of Physical Chemistry Letters, 11, 5100–5107.

[11] Krishna, A., Gottis, S., Nazeeruddin, M.K. and Sauvage, F., (2019), Mixed dimensional 2D/3D hybrid perovskite absorbers: the future of perovskite solar cells?, Advanced Functional Materials, 29, 1806482.

[12] Zhang, Y., Lyu, M., Qiu, T., Han, E., Kim, I.K., Jung, M.-C., Ng, Y.H., Yun, J.-H. and Wang, L., (2020), Halide perovskite single crystals: optoelectronic applications and strategical approaches, Energies, 13, 4250.

[13] Trivedi, S., Prochowicz, D., Parikh, N., Mahapatra, A., Pandey, M.K., Kalam, A., Tavakoli, M.M. and Yadav, P., (2021), Recent progress in growth of single-crystal perovskites for photovoltaic applications, ACS Omega, 6, 1030–1042.

[14] Pham, P. V., Bodepudi, S.C., Shehzad, K., Liu, Y., Xu, Y., Yu, B. and Duan, X., (2022), 2D heterostructures for ubiquitous electronics and optoelectronics: principles, opportunities, and challenges, Chemical Reviews, 122, 6514–6613.

[15] Wang, J., Li, J., Lan, S., Fang, C., Shen, H., Xiong, Q. and Li, D., (2019), Controllable growth of centimeter-sized 2D perovskite heterostructures for highly narrow dual-band photodetectors, ACS Nano, 13, 5473–5484.

[16] Cheng, X., Han, Y. and Cui, B., (2022), Fabrication strategies and optoelectronic applications of perovskite heterostructures, Advanced Optical Materials, 10, 2102224.

[17] Cao, F., Li, Z., Liu, X., Shi, Z. and Fang, X., (2022), Air induced formation of Cs3Bi2Br9/Cs3BiBr6 bulk heterojunction and its dual- band photodetection abilities for light communication, Advanced Functional Materials, 32, 2206151.

[18] Hwang, B. and Lee, J., (2019), 2D perovskite based self- aligned lateral heterostructure photodetectors utilizing vapor deposition, Advanced Optical Materials, 7, 1801356.

[19] Wang, J., Li, J., Tan, Q., Li, L., Zhang, J., Zang, J., Tan, P., Zhang, J. and Li, D., (2017), Controllable synthesis of two-dimensional ruddlesden–popper type perovskite heterostructures, The Journal of Physical Chemistry Letters, 8, 6211–6219.

[20] Li, J., Han, Z., Gu, Y., Yu, D., Liu, J., Hu, D., Xu, X. and Zeng, H., (2021), Perovskite single crystals: synthesis, optoelectronic properties, and application, Advanced Functional Materials, 31, 2008684.

[21] Liu, J., Xue, Y., Wang, Z., Xu, Z.-Q., Zheng, C., Weber, B., Song, J., Wang, Y., Lu, Y., Zhang, Y. and Bao, Q., (2016), Two-dimensional CH3NH3PbI3 perovskite: synthesis and optoelectronic application, ACS Nano, 10, 3536–3542.

[22] Protesescu, L., Yakunin, S., Nazarenko, O., Dirin, D.N. and Kovalenko, M. V., (2018), Low-cost synthesis of highly luminescent colloidal lead halide perovskite nanocrystals by wet ball milling,

ACS Applied Nano Materials, 1, 1300–1308.

[23] Zhu, T. and Gong, X., (2021), Low- dimensional perovskite materials and their optoelectronics, InfoMat, 3, 1039–1069.

[24] Poglitsch, A. and Weber, D., (1987), Dynamic disorder in methylammoniumtrihalogenoplumbates (II) observed by millimeter- wave spectroscopy, The Journal of Chemical Physics, 87, 6373–6378.

[25] Raghavan, C.M., Chen, T.-P., Li, S.-S., Chen, W.-L., Lo, C.-Y., Liao, Y.-M., Haider, G., Lin, C.-C., Chen, C.-C., Sankar, R., Chang, Y.-M., Chou, F.-C. and Chen, C.-W., (2018), Low-threshold lasing from 2D homologous organic–inorganic hybrid ruddlesden–popper perovskite single crystals, Nano Letters, 18, 3221–3228.

[26] Stoumpos, C.C., Cao, D.H., Clark, D.J., Young, J., Rondinelli, J.M., Jang, J.I., Hupp, J.T. and Kanatzidis, M.G., (2016), Ruddlesden–popper hybrid lead iodide perovskite 2D homologous semiconductors, Chemistry of Materials, 28, 2852–2867.

[27] Wang, K., Wu, C., Yang, D., Jiang, Y. and Priya, S., (2018), Quasi-two-dimensional halide perovskite single crystal photodetector, ACS Nano, 12, 4919–4929.

[28] Klein-Kedem, N., Cahen, D. and Hodes, G., (2016), Effects of light and electron beam irradiation on halide perovskites and their solar cells, Accounts of Chemical Research, 49, 347–354.

[29] Xiao, C., Li, Z., Guthrey, H., Moseley, J., Yang, Y., Wozny, S., Moutinho, H., To, B., Berry, J.J., Gorman, B., Yan, Y., Zhu, K. and Al-Jassim, M., (2015), Mechanisms of electron-beam-induced damage in perovskite thin films revealed by cathodoluminescence spectroscopy, The Journal of Physical Chemistry C, 119, 26904–26911.

[30] Kim, T.W., Shibayama, N., Cojocaru, L., Uchida, S., Kondo, T. and Segawa, H., (2018), Real-time in situ observation of microstructural change in organometal halide perovskite induced by thermal degradation, Advanced Functional Materials, 28, 1804039.

[31] Ran, J., Dyck, O., Wang, X., Yang, B., Geohegan, D.B. and Xiao, K., (2020), Electron beam related studies of halide perovskites: challenges and opportunities, Advanced Energy Materials, 10, 1903191.

[32] Rothmann, M.U., Li, W., Zhu, Y., Liu, A., Ku, Z., Bach, U., Etheridge, J. and Cheng, Y., (2018), Structural and chemical changes to CH3NH3PbI3 induced by electron and gallium ion beams, Advanced Materials, 30, 1800629.

[33] Zhou, J., Chu, Y. and Huang, J., (2016), Photodetectors based on two-dimensional layer-structured hybrid lead iodide perovskite semiconductors, ACS Applied Materials & Interfaces, 8,

25660–25666.

[34] Xu, Y., Li, Y., Wang, Q., Chen, H., Lei, Y., Feng, X., Ci, Z. and Jin, Z., (2022), Two-dimensional BA2PbBr4-based wafer for X-rays imaging application, Materials Chemistry Frontiers, 6, 1310–1316.

[35] Lin, J., Chen, D., Wu, C., Hsu, C., Chien, C., Chen, H., Chou, P. and Chiu, C., (2021), A universal approach for controllable synthesis of n- specific layered 2D perovskite nanoplates, Angewandte Chemie International Edition, 60, 7866–7872.

[36] Choi, E., Zhang, Y., Soufiani, A.M., Lee, M., Webster, R.F., Pollard, M.E., Reece, P.J., Lee, W., Seidel, J., Lim, J., Yun, J.-H. and Yun, J.S., (2022), Exploration of sub-bandgap states in 2D halide perovskite single-crystal photodetector, Npj 2D Materials and Applications, 6, 43.

[37] Miao, Y., Xiao, Z., Zheng, Z., Lyu, D., Liu, Q., Wu, J., Wu, Y., Wen, X., Shui, L., Hu, X., Wang, K., Tang, Z. and Jiang, X., (2022), Designable layer edge states in quasi- 2D perovskites induced by femtosecond pulse laser, Advanced Science, 9, 2201046.

[38] Du, Q., Zhu, C., Yin, Z., Na, G., Cheng, C., Han, Y., Liu, N., Niu, X., Zhou, H., Chen, H., Zhang, L., Jin, S. and Chen, Q., (2020), Stacking effects on electron–phonon coupling in layered hybrid perovskites via microstrain manipulation, ACS Nano, 14, 5806–5817.